Astron. Astrophys. 333, 38–42 (1998)

ASTRONOMY AND ASTROPHYSICS

Millimeter-wave thermal dust emission from luminous mergers

J. Braine[1] **and M. Dumke**[2,3]

[1] Observatoire de Bordeaux, URA 352, CNRS/INSU, B.P. 89, F-33270 Floirac, France
[2] Max-Planck-Institut für Radioastronomie, Auf dem Hügel 69, D-53121 Bonn, Germany
[3] Institut de Radioastronomie Millimétrique, 300 rue de la Piscine, F-38406 St. Martin d'Hères Cedex, France

Received 13 November 1997 / Accepted 2 January 1998

Abstract. We have observed several infrared-luminous galaxies which are in the process of merging (Mkn 231, Arp 299, NGC 6240, NGC 520, and IRAS 17208-0014) at $1.2\,\mathrm{mm}$ with the multi-channel bolometer at the IRAM 30-meter telescope. Such observations of the long-wavelength thermal dust emission provide an alternative to CO as a measure of the gas mass.

Comparing the masses of gas determined from the dust emission and from CO observations of these galaxies, we find that the conversion factor $N(\mathrm{H_2})/I_{\mathrm{CO}(1-0)} \lesssim 0.5\ 10^{20}\,\mathrm{cm^{-2}(\,K\,km\,s^{-1})^{-1}}$. Our calculations are conservative. We have chosen a ν^2 emissivity; other emission laws result in higher dust temperatures. We have made our calculations assuming a metallicity of $2Z_\odot$, which is low for a galactic nucleus. We have not assumed any enhancement of the dust emission through agglomeration of dust particles nor destruction of grains. Finally, we have assumed that all of the gas associated with 1.2mm thermal dust emission is molecular. Expected deviations from these assumptions would *all* decrease the gas masses estimated from the thermal dust emission, resulting in even lower values for the $N(\mathrm{H_2})/I_{\mathrm{CO}}$ conversion factor.

Key words: galaxies: individual: Mkn 231, NGC 520, NGC 6240, Arp 299 – galaxies: ISM – radio continuum: galaxies

1. Introduction

Whatever their source of power, starburst or active nucleus or both, IR-luminous galaxies have extremely strong CO emission. The mass of molecular gas deduced from the CO emission is typically several $10^{10}\,\mathrm{M_\odot}$ for the brightest sources. The motivation for the present work is to provide an independent check to the neutral gas masses derived from CO observations. These are not the first millimeter observations of IR-luminous galaxies but past results have been controversial and the technical advances make re-doing the observations worthwhile.

The reason for observing the long-wavelength tail of the thermal dust emission is that the temperature dependence is minimized. As an example, suppose that a given region has a measured 100μ flux of $50\,\mathrm{Jy}$. This corresponds to a gas mass (calculated as described in Sect. 3) of $5\,10^8\,\mathrm{M_\odot}$ if the dust is at $30\,\mathrm{K}$. For $20\,\mathrm{K}$ dust, however, the mass would be more than 10 times greater. Even at 350μ, a flux of $4\,\mathrm{Jy}$ corresponds to $5\,10^8\,\mathrm{M_\odot}$ of gas if the dust is at $30\,\mathrm{K}$ but 5 times as much if the temperature is $15\,\mathrm{K}$ and still more than twice as much at $20\,\mathrm{K}$. At $1.22\,\mathrm{mm}$, the effect is half that at 350μ. These differences are not linked to the behavior of the dust grains but strictly to the form of the Planck function.

Fig. 1 shows the increase in emission at a given frequency as the temperature changes. At low temperatures even a slight variation results in a large change in the flux at 100μm. At 350μm and 450μm the temperature sensitivity is still high up to temperatures of about 40 and 30 K respectively. Near wavelengths of $\sim 1\,\mathrm{mm}$, however, the emission varies virtually linearly with the temperature above 12–20 K, so that even an uncertainty of 25% in the temperature only yields a ∼25% uncertainty in the gas mass. Temperature-based errors are thus minor at $1\,\mathrm{mm}$ but dominant at 100μm.

2. Observations and results

The observations were all made with the 19-channel MPIfR bolometer mounted on the IRAM 30meter telescope on Pico Veleta (Granada, Spain). The central frequency and bandwidth are $245\,\mathrm{GHz}$ and $\sim 70\,\mathrm{GHz}$ respectively (cf. Guélin et al. 1995) and the beam size is roughly $11''$ (cf. Braine et al. 1997). We refer to the $1.2\,\mathrm{mm}$ emission but use the more precise value of $245\,\mathrm{GHz}$ in all calculations. The sources were mapped in the on-the-fly mode except for 17208-0014 which was only observed in on-off mode. Mkn 231 and NGC 6240 were also observed in on-off mode.

First-order baselines were subtracted and then, to reduce weather-related sky noise, noise correlated from one channel to another was subtracted. The maps were then restored, converted to equatorial coordinates, and combined. For the ON-OFF observations, the average value of the non-central pixels (channels) was subtracted from the central channel in order to reduce weather-related fluctuations. ON-OFF observations were only carried for sources smaller than the separation between two channels ($\sim 20''$).

Maps of the $1.2\,\mathrm{mm}$ emission superposed on Digital Sky Survey images of Mkn 231, NGC 520, and Arp 299 are shown

Send offprint requests to: Jonathan Braine

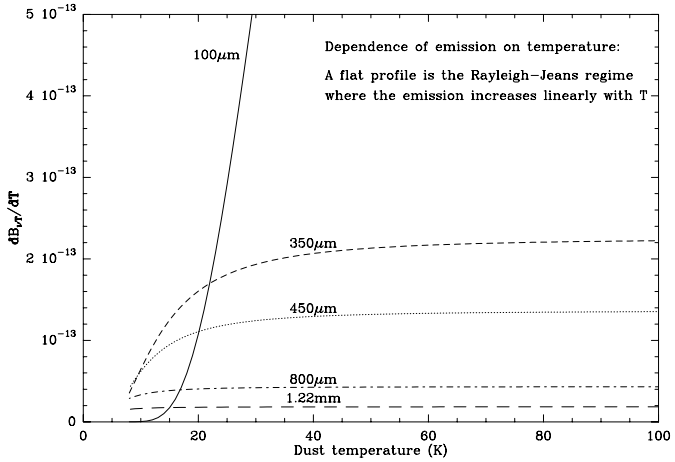

Fig. 1. $\delta B_{\nu,T}/\delta T$ versus T, the dust temperature for 5 wavelengths – 100μm, 350μm, 450μm, 800μm, and $1.22\,\mathrm{mm}$. We see that the shorter the wavelength, the greater the sensitivity to the dust temperature. Given that the dust temperature is not known with precision and is certainly a mix of many temperatures along any line of sight, it is important to minimize the temperature dependence if one is to measure the mass of gas. Long wavelengths ($\sim 1\,\mathrm{mm}$) are necessary for cool dust.

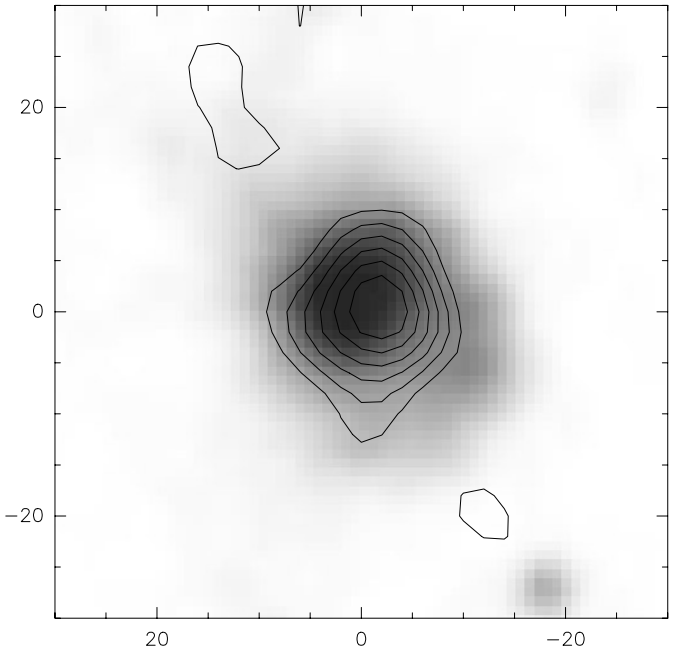

Fig. 2. Mkn 231: grey scale is optical image from the Digital Sky Survey; contours are the total $1.2\,\mathrm{mm}$ emission. First contour is at $5\,\mathrm{mJy\,beam^{-1}}$ and further contours are separated by $5\,\mathrm{mJy\,beam^{-1}}$. Offsets are in arcseconds with respect to the position given in Table 1. Note that the center of the mm continuum emission is at the radio position (Condon et al. 1991a,b) and not the (0,0) position of this map.

in Figs. 2, 4, and 5. Poor weather forced us to stop observing NGC 6240; no map is shown because of the poor image quality.

The $1.2\,\mathrm{mm}$ emission in the bolometer band is the sum of the thermal dust emission (what we want to measure), synchrotron, free-free, and line emission - essentially the CO(2–1) line. To this end, we estimate spectral indices of the synchrotron emission and, when enough data are present, the fraction of free-free emission and the total contribution in the bolometer band. To estimate the flux from the CO(2–1) line in the bolometer band, we take CO(2–1) observations with the IRAM 30meter telescope when possible (similar beamsize) or try to estimate the CO(2–1) flux within the bolometer beam from interferometric CO(1–0) observations. In the latter case (NGC 520 and IRAS 17208-0014), we assume an intrinsic CO($\frac{2-1}{1-0}$) ratio of 0.7 (Radford et al. 1991). The line contribution to the observed $1.2\,\mathrm{mm}$ emission may be higher than what we estimate for the CO(2–1) line because other lines such as ^{13}CO (2–1) or HCN(3–2) may contribute.

With the exception of Mkn 231, the thermal dust emission is the major component of the flux detected in the bolometer band. Reasonable errors in the other contributions would not have a significant effect on the results presented here. In particular, we have assumed a fairly low fraction of free-free emission in order not to overestimate the contribution of the "radio" fluxes to the 1.2 mm emission. All calculations are made with the thermal dust emission alone, after subtraction of the synchrotron, free-free, and line contributions.

Table 1 provides the central coordinates for the maps and the positions observed in on-off mode. Also included are the FIR luminosities, assumed distances, and the breakdown of the different components of the emission detected in the bolometer band. The last columns in Table 1 indicate the chopper throw and its position angle (measured North to East) for non-pointlike sources. The sensitivity decreases for emission extended beyond the chopper throw in the direction of the chop. We chose to observe the sources at hour angles such that the chopper throw was roughly aligned with the minor axis. The amount of flux lost is probably very small but we prefer not to give total fluxes for extended sources nor compare with regions larger than the chopper throw. The gas mass estimates are given in Table 2. Comparison of dust-based and CO-based estimates provide an immediate assessment of the $N(\mathrm{H_2})/I_{\mathrm{CO}}$ ratio.

2.1. Mkn 231

The synchrotron emission from Mkn 231 is variable on a time scale of years (Condon et al. 1991a). We therefore use the highest cm-wave measurement (Condon et al. 1991a Oct. 1987) and the recent $109\,\mathrm{GHz}$ measurement by Bryant & Scoville (1996). The spectral index is $\alpha = -0.7$. It is clear that Mrk 231 is an exceptional object (Condon et al. 1991b) and that the radio emission is too strong to come only from the starburst. In order to avoid oversubtracting the amount of synchrotron/free-free emission, we have assumed that no thermal (free-free) emission was present.

The very weak thermal dust emission at $1.2\,\mathrm{mm}$ shows that the dust temperature must be very high. More importantly, *it is not possible to fit the spectrum with a dust emissivity varying more slowly than* ν^2. A plausible single temperature fit is with

Table 1. Sources and central coordinates (B1950) of maps presented here, assumed distance in Mpc, Far-Infrared flux from Soifer et al. (1989) IRAS data unless otherwise indicated. The last two columns indicate the chopper throws used and, except for the point sources, the position angle of the chopping direction. NGC 3690 and IC 694 are the western and eastern parts of Arp 299. The contribution of the CO(2–1) line to the $1.2\,\mathrm{mm}$ emission is estimated from the values given in Table 2.
a: Young et al. (1989) for IRAS flux densities. b: Martin et al. (1989) for IRAS flux densities.
c: over roughly two bolometer beam areas.

Source	R.A. B1950	Dec B1950	Dist. Mpc	$L_{40-122\mu}$ $\mathrm{L}_\odot$	sync+f-f mJy	$S_{\mathrm{CO}(2-1)}$ mJy	S_{dust} mJy	Chop $''$	PA $^\circ$
Mkn 231	12:54:05.1	57:08:38	253	$3\,10^{12}$	28	2	7.5	32	
NGC 520	01:21:59.6	03:31:53	43	$9\,10^{10}$	10	6	34	44	44, 50, 57, 61
NGC 6240[a]	16:50:27.7	02:28:58	147	$7\,10^{11}$	12.5	4	20.5	32	-47, -43
17208-0014[b]	17:20:47.87	-00:14:15.6	257	$3\,10^{12}$	3	5	28	32	
Arp 299	11:25:42.8	58:50:17	62	$7\,10^{11}$				32	-35, -8, -13, -30, -48
NGC 3690				$3\,10^{11}$	5	7[c]	38[c]		
IC 694				$4\,10^{11}$	13	9[c]	78[c]		

Table 2. The CO(2-1) fluxes are as observed at the IRAM 30-meter telescope or estimated as described in Sect. 3; NGC 3690 and IC 694 are not separated by single-beam CO(1–0) observations. The dust temperatures are *lower* limits – other emissivity laws yield higher dust temperatures. $M_{\mathrm{gas_{dust}}}$ and $M_{\mathrm{gas_{co}}}$ are the dust-based and CO-based gas masses calculated as described in Sects. 3.2 and 3.1 respectively from the CO(2–1) and then CO(1–0) data. $S_{\mathrm{dust,int}}$ is the $1.2\,\mathrm{mm}$ flux density integrated over the source (same as in Table 1 for a point source). The last two columns give the estimated upper limits to the $N(\mathrm{H_2})/I_{\mathrm{CO}(2-1)}$ and $N(\mathrm{H_2})/I_{\mathrm{CO}(1-0)}$ factors in units of $10^{20}\,\mathrm{cm^{-2}(\,K\,km\,s^{-1})^{-1}}$.
a: Radford et al. (1991). b: Sanders et al. (1988). c: Combes et al. (1991). d: Planesas et al. (1991).
e: Estimated from Casoli et al. (1989), converted to main beam brightness over the equivalent of a $\sim 16''$ beam.
f: Mirabel et al. (1990)

Source	CO(2–1) $\mathrm{K\,km\,s^{-1}}$	T_{dust} K	$M_{\mathrm{gas_{dust}}}$ $\mathrm{M}_\odot$	$M_{\mathrm{gas_{co}}}$ $\mathrm{M}_\odot$	CO(1–0) $\mathrm{K\,km\,s^{-1}}$	beam $''$	$S_{\mathrm{dust,int}}$ mJy	$M_{\mathrm{gas_{dust}}}$ $\mathrm{M}_\odot$	$M_{\mathrm{gas_{co}}}$ $\mathrm{M}_\odot$	$N(\mathrm{H_2})/I_{\mathrm{CO}}$ 2–1	1–0
Mkn 231	42[a]	68	$5.0\,10^9$	$2.3\,10^{10}$	22[a]	22	7.5	$5.0\,10^9$	$4.0\,10^{10}$	0.2	0.1
NGC 520	108[b]	33	$1.5\,10^9$	$1.4\,10^9$	45[b]	45	76	$3.2\,10^9$	$9.8\,10^9$	1.1	0.3
NGC 6240	76[c]	33	$1.0\,10^{10}$	$1.4\,10^{10}$	61[b]	22	37	$1.8\,10^{10}$	$3.7\,10^{10}$	0.7	0.5
17208-0014	91[d]	34	$4.3\,10^{10}$	$4.2\,10^{10}$	7[f]	55	28	$4.3\,10^{10}$	$8.2\,10^{10}$	1.0	0.5
Arp 299											
NGC 3690	63[e]	32	$3.6\,10^9$	$3.6\,10^9$		$\sim$16	38			1.0	
IC 694	81[e]	30	$7.9\,10^9$	$4.6\,10^9$		$\sim$16	78			1.7	

a dust temperature of about $70\,\mathrm{K}$, emissivity varying as ν^2, and becoming optically thick at about 120μ (*i.e.* Downes et al. 1993).

2.2. NGC 520

NGC 520 is a much closer galaxy with some extended CO emission. The IRAS observations encompass the entire system and thus may mix warm gas in the central area with somewhat cooler material further out (which probably would not contribute much to the IRAS fluxes). Nonetheless, the IRAS fluxes are "warm" – $S_{60\mu}/S_{100\mu} \sim 2/3$, which is roughly twice the ratio in "normal" galaxies. Radio data are from Condon et al. (1990) and Urbanik et al. (1985) who find a synchrotron spectrum of $-0.62 \pm .06$; we have assumed a thermal fraction of 10% at $10\,\mathrm{GHz}$. In NGC 520, the contributions from CO, synchrotron, and probably free-free emission are within the normal range.

2.3. NGC 6240

NGC 6240 is very luminous with two central sources separated by $\sim 2''$ (Condon et al. 1982; Schulz et al. 1993). They are assumed to be the remnants of the nuclei of the pre-merger galaxies. The IRAS fluxes are very "warm" – $S_{60\mu}/S_{100\mu} \sim 0.9$. Radio data at 1.49, 4.6, and 8.1 GHz are from Colbert et al. (1994); a synchrotron spectral index of -0.8 and a thermal fraction of 10% at $10\,\mathrm{GHz}$ provide a good fit to the data.

2.4. IRAS 17208-0014

Despite its huge luminosity, few observations of this source are available. Martin et al. (1989) measured an 18 cm flux of 90 ± 15 mJy and we have assumed a synchrotron spectral index of -0.8 and a thermal fraction of 10% at $10\,\mathrm{GHz}$. The CO data are from Planesas et al. (1991) and Mirabel et al. (1990).

2.5. Arp 299

Following Joy et al. (1989), we will assume that 60% of the FIR radiation at $\lambda \gtrsim 50\mu$ can be attributed to IC 694 (Arp 299 East) and 40% to the two parts of Arp 299 West (NGC 3690). We evaluate the amount of synchrotron and free-free radiation from Aalto et al. (1997), who detect the continuum at $110\,\mathrm{GHz}$ and whose results are consistent with Gehrz et al. (1983). It is worth noting that our results differ markedly with Aalto et al.'s ^{13}CO

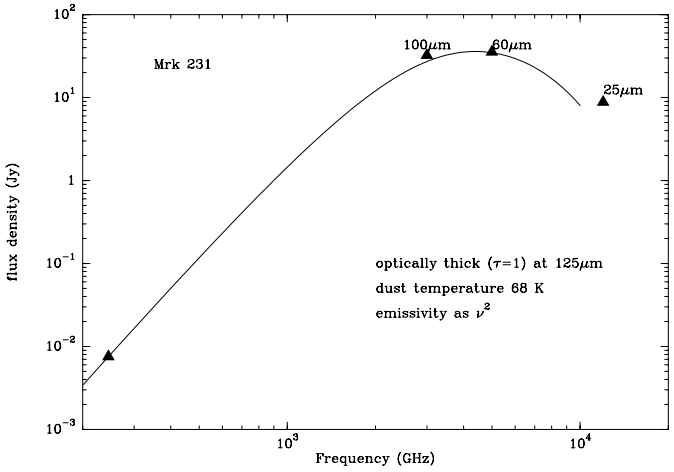

Fig. 3. Approximate fit to the FIR/mm thermal dust spectrum of Mkn 231. Only quite warm dust is necessary and the dust is optically thick at $\lambda \sim 100\mu$m. This implies very high column densities, consistent with the point-like appearance of the CO and radio continuum (Condon et al. 1991a) emission. The $1.2\,\mathrm{mm}$ emission is not extended at our resolution ($fwhm_{\mathrm{mkn231}} \sim 11'' \approx fwhm_{\mathrm{beam}}$). The 100μm point cannot be fit by adding cool dust.

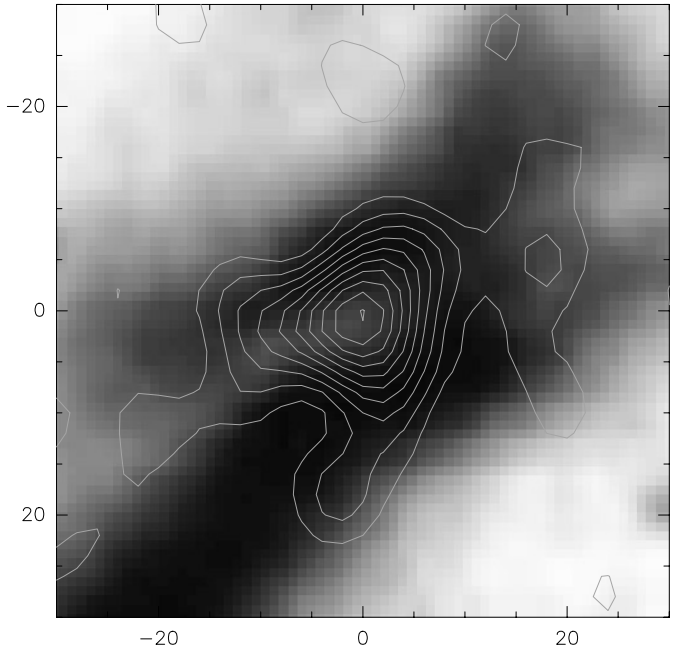

Fig. 4. NGC 520: grey scale is optical image from the Digital Sky Survey; contours are the total $1.2\,\mathrm{mm}$ emission. First contour is at $5\,\mathrm{mJy\,beam^{-1}}$ and further contours are separated by $5\,\mathrm{mJy\,beam^{-1}}$. Offsets are in arcseconds with respect to the position given in Table 1.

results which could be expected to trace the gas column density much like the dust emission presented here. The CO data come from Casoli et al. (1989) who observed with a beam similar to ours. A substantial error in any of these quantities will not change our results because it is the thermal dust emission which dominates. Even a 30% error on the amount of synchrotron and free-free emission or CO flux produces a change in the amount

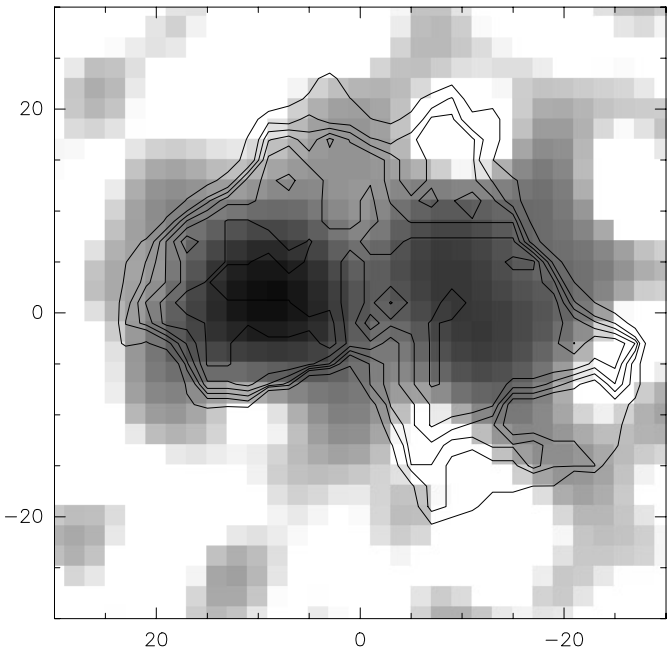

Fig. 5. Arp 299: grey scale is total $1.2\,\mathrm{mm}$ emission and contours are the high-brightness part of the optical image from the Digital Sky Survey. Offsets are in arcseconds with respect to the position given in Table 1.

of thermal dust emission at $1.2\,\mathrm{mm}$ which is well within the uncertainties due to calibration and the boundary of the source. Whatever the corrections due to the other sources of emission, IC 694 emits roughly twice as strongly at $1.2\,\mathrm{mm}$ as NGC 3690, both in integrated emission and in peak flux density per beam. It is interesting that the obscuring dust and the blue light have such similar morphologies in the high-brightness regions. In contrast, the $1.2\,\mathrm{mm}$ maximum of NGC 520 corresponds to an optical minimum, showing that some of the dust acts as a screen.

3. Molecular gas masses

3.1. From CO observations

The gas mass in molecular clouds can be calculated as follows:

$$M_{\mathrm{gas_{co}}} = \Omega\, D^2\, I_{\mathrm{co}}\, N(\mathrm{H_2})/I_{\mathrm{CO}}\, 2 m_p f_{\mathrm{H}}^{-1}$$

where Ω is the beam solid angle ($\int 2\pi\theta \exp(-\frac{4\ln(2)\theta^2}{\theta_{fwhm}} d\theta$), D is the distance, I_{co} is the CO flux in $\mathrm{K\,km\,s^{-1}}$, $N(\mathrm{H_2})/I_{\mathrm{CO}}$ is the conversion factor, and m_p and f_{H} are the proton mass and the hydrogen fraction of gas by mass. To simplify calculations, we take $N(\mathrm{H_2})/I_{\mathrm{CO}} = 10^{20}\,\mathrm{cm^{-2}}(\,\mathrm{K\,km\,s^{-1}})^{-1}$ for both transitions. Because we then use the dust emission to place an upper limit on this ratio, the value we use to obtain the "CO-based" gas mass has no influence on the conclusions of this work.

3.2. From the 1.2 mm thermal dust emission

The first step is to subtract the synchrotron, free-free, and CO(2–1) line contributions, leaving only the thermal dust emission

as found in column 8 of Table 1 and col. 8 of Table 2. The basic procedure is to fit grey-body curves to the thermal dust emission at $1.2\,\mathrm{mm}$ combined with the IRAS 100μ, 60μ, and 25μ fluxes. Single temperature fits are generally impossible (see however discussion of Mkn 231) so we fit two grey body curves at different temperatures. More than two temperatures would be unconstrained. In practice, we assume the $1.2\,\mathrm{mm}$ emission is generated by the cooler gas and that the 25μ emission comes from the warmer component. These assumptions are much less precarious than the temperatures or the fluxes themselves. This provides the normalization for the curves and the temperatures are fit to the 100μ and 60μ data points. About 99% of the gas mass is in the lower temperature component.

To convert the fits into gas masses, we take the Draine & Lee (1984) cross-section of dust per H-atom and assume that the metallicity is twice that of the local diffuse medium studied by Draine & Lee.

$$M_{\mathrm{gas}_{\mathrm{dust}}} = \frac{D^2\, S_{\mathrm{dust}}\, m_p}{\sigma\, B_{\nu,T}\, f_{\mathrm{H}}} \quad \text{where}$$

$$\sigma = 9.2\,10^{-27}\,\frac{1.22\,\mathrm{mm}^2}{\lambda}\,\frac{b}{1}\,\frac{Z}{2Z_\odot}\,\mathrm{cm}^{-2}$$

This amounts to doubling their cross-sections.

3.3. Results and conclusions

Table 2 presents the gas masses as calculated from the various observations. For NGC 520 and NGC 6240, both central and integrated values for the thermal dust emission are given and compared with CO data of appropriate resolution. For the two sources in Arp 299, only integrated values were given because the CO(2–1) observations were not centered on the two peaks individually. The last columns give the upper limits to the $N(\mathrm{H}_2)/I_{\mathrm{CO}}$ values determined by setting the CO-based gas masses equal to the upper limits to the dust-based gas masses. In equation form, this is

$$N(\mathrm{H}_2)/I_{\mathrm{CO}} = \frac{S}{2\Omega I_{\mathrm{co}}\,\sigma B_{\nu,T}}\,\frac{\mathrm{cm}^{-2}}{\mathrm{K\,km\,s^{-1}}}$$

The upper limit to the $N(\mathrm{H}_2)/I_{\mathrm{CO}}$ ratio varies from about 0.5 – $1\times10^{20}\,\mathrm{cm}^{-2}(\,\mathrm{K\,km\,s^{-1}})^{-1}$ in all sources with the exception of Mkn 231 where it is clearly lower.

On average, these upper limits are a factor several below the conversion factors that have typically been used for interacting galaxies. Molecular gas masses of merging galaxies estimated from CO observations are probably overestimated by a factor 3 – 10 (for a typical $N(\mathrm{H}_2)/I_{\mathrm{CO}(1-0)} = 2\,10^{20}\,\mathrm{cm}^{-2}(\,\mathrm{K\,km\,s^{-1}})^{-1}$).

We would like to stress that the "dust-based gas masses" are upper limits rather than estimates because of the following points.

(1) We have not tried to subtract emission due to dust in the atomic gas. Subtracting any such contribution would reduce the amount of molecular gas (and thus the $N(\mathrm{H}_2)/I_{\mathrm{CO}}$ factor) we estimate.

(2) We have assumed a ν^2 emissivity law up to $\lambda \lesssim 100\mu$m, following Draine & Lee 1984. Had we calculated dust temperatures from a $\nu^{1.5}$ or discontinuous emissivity as in Hildebrand (1983), the dust temperatures we determine would be higher and our gas mass estimates correspondingly lower.

(3) We have not assumed a high metallicity even though we have observed the centers of massive systems. Had we assumed the metallicity and grain properties of Mauersberger et al. (1996) or Guélin et al. (1995) for NGC 253 and M 51 respectively, our limits would be a factor 3 lower.

The observations presented here lend further support to the idea that gas masses in mergers have been overestimated.

Acknowledgements. We gratefully acknowledge use of the SkyView data base maintained by HEASARC at the NASA GSFC.

References

Aalto, S., Radford S.J.E., Scoville N.Z., Sargent A.I. 1997, ApJ 475, L107
Braine, J., Guélin, M., Dumke, M., et al. 1997 A&A 326, 963
Bryant, P.M., & Scoville, N.Z. 1996 ApJ 457, 678
Casoli, F., Combes, F., Augarde, R., Figon, P., Martin, J.-M. 1989 A&A 224, 31
Colbert E.J.M., Wilson A.S., Bland-Hawthorn J. 1994, ApJ 436, 89
Combes, F., Casoli, F., Encrenaz, P., Gerin, M., Laurent, C. 1991 A&A 248, 607
Condon, J.J., Condon, M.A., Gisler, G., Puschell, J.J. 1982 ApJ 252, 102
Condon, J.J., Frayer, D.T., Broderick J.J. 1991a ApJ 101, 362
Condon, J.J., Huang, Z.-P., Yin, Q.F., Thuan, T.X. 1991b, ApJ 378, 65
Condon, J. J., *et al.* 1990, ApJS, 73, 359
Downes, D., Solomon, P.M., Radford, S.J.E. 1993, ApJ 414, L13
Draine, B.T., Lee, H.M. 1984, ApJ 285, 89
Gehrz R.D., Sramek R.A., Weedman D.W. 1983, ApJ 267, 551
Guélin, M., Zylka, R., Mezger, P.G. Haslam, C.G.T., Kreysa, E. 1995, A&A 298, L29
Hildebrand, R.H. 1983, QJRAS 24, 267
Joy, M., Lester D.F., Harvey P.M. et al 1989 ApJ 339, 100
Martin, J.-M., Le Squeren A.M., Bottinelli L., Gougenheim L., Dennefeld M. 1989 A&A 208, 39
Mauersberger, R., Henkel, C., Wielebinski, R., Wiklind, T., Reuter H.-P. 1996, A&A 305, 421
Mirabel I.F., Booth R.S., Johansson L.E.B., Garay G., Sanders D.B. 1990, A&A 236, 327
Planesas, P., Mirabel, I.F., Sanders, D.B. 1991, ApJ 370, 172
Radford, S.J.E., Solomon, P.M., Downes, D. 1991, ApJ 368, L15
Sanders, D.B., Soifer, B.T., Scoville, N.Z., Sargent A.I. 1988 ApJ 324, L55
Schulz H., Fried J.W., Roser S., Keel W.C. 1993 A&A 277, 416
Soifer, B.T., Boehmer L., Neugebauer G., Sanders, D. 1989 AJ 98, 766
Urbanik M., Gräve R., Klein U. 1985, A&A 152, 291.
Young J.S., Xie S., Kenney J.D.P., Rice W.L. 1989, ApJS 70, 699